

A One-Dimensional Particle-in-Cell Model of Plasma Build-Up in Vacuum Arcs

H. Timko^{*1,2}, K. Matyash³, R. Schneider³, F. Djurabekova², K. Nordlund², A. Hansen¹, A. Descoeudres¹, J. Kovermann¹, A. Grudiev¹, W. Wuensch¹, S. Calatroni¹, and M. Taborelli¹

¹ CERN, Genève 23, CH-1211, Switzerland

² Helsinki Institute of Physics and Department of Physics, P. O. Box 43, FIN-00014 University of Helsinki, Finland

³ Max-Planck-Institut für Plasmaphysik, EURATOM Association, Wendelsteinstrasse 1, D-17491, Greifswald, Germany

Received 3 March 2010, accepted 9 March 2010

Published online 5 January 2011

Key words Vacuum arcs, electrical discharges, plasma build-up, PIC simulations.

Understanding the mechanism of plasma build-up in vacuum arcs is essential in many fields of physics. A one-dimensional particle-in-cell computer simulation model is presented, which models the plasma developing from a field emitter tip under electrical breakdown conditions, taking into account the relevant physical phenomena. As a starting point, only an external electric field and an initial enhancement factor of the tip are assumed. General requirements for plasma formation have been identified and formulated in terms of the initial local field and a critical neutral density. The dependence of plasma build-up on tip melting current, the evaporation rate of neutrals and external circuit time constant has been investigated for copper and simulations imply that arcing involves melting currents around $0.5 - 1 \text{ A}/\mu\text{m}^2$, evaporation of neutrals to electron field emission ratios in the regime $0.01 - 0.05$, plasma build-up timescales in the order of $\sim 1 - 10 \text{ ns}$ and two different regimes depending on initial conditions, one producing an arc plasma, the other one not. Also the influence of the initial field enhancement factor and the external electric field required for ignition has been explored, and results are consistent with the experimentally measured local field value of $\sim 10 \text{ GV/m}$ for copper.

© 2011 WILEY-VCH Verlag GmbH & Co. KGaA, Weinheim

1 Introduction

In many areas of research, from fusion reactors [1] to satellite systems [2], one is confronted with the issue of electrical discharges, especially with vacuum arcs. Gaining a deeper knowledge of the mechanism of these arcs is thus desirable. Based on cathode phenomena, three phases of an arc can be distinguished [3], we call these (i) the onset of arcing, during which electron emission is triggered, (ii) the burning of the arc, during which the plasma is created and maintained, and (iii) the surface modification (cratering) of the cathode subsequent to it. The particle-in-cell (PIC) code presented here has been developed to model the plasma build-up in vacuum arcs, which is the early stage of the burning of an arc.

Linear collider designs such as the Compact Linear Collider (CLIC) call for a high accelerating gradient, that raises the problem of breakdowns in ultra high vacuum also in radio frequency (RF) accelerating cavities [4]. To complement high gradient RF experiments, an experimental programme to explore the nature of breakdowns is under way in a direct current (DC) setup at CERN [5, 6], which aims at more detailed studies of sparks under simplified conditions. This DC setup served as a basis of comparison between theory and experiment.

A 1d3v PIC code is used for simulations, meaning that no side losses of the plasma can be resolved and particle motion is characterised by one spatial coordinate (1d) and three velocity components (3v). The 1d simplification is motivated by the cylindrical symmetry of the geometry of DC experiments: The development of arcs is restricted to a small and well defined area between locally plane electrodes, with an electric field perpendicular to these. The aim is to simulate the build-up of electron, neutral and ion densities. Two different mechanisms have been suggested to produce the explosive electron emission [7, 8] needed for the formation of

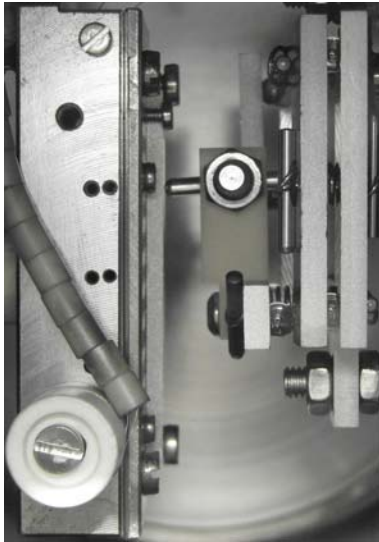
* Corresponding author: E-mail: helga.timko@helsinki.fi, Phone: +41 22 76 74769

the arc plasma: Electron emission due to (i) micro-protrusions (field emitting tips) on the cathode surface [9, 3] and due to (ii) insulating particles resting on or embedded in a metal substrate [10]. In our model, a field emitting tip is assumed in terms of properties such as the field enhancement factor, although the tip itself is not modelled. Resolvable physical quantities are areal densities such as current density. Thus one can interpret this one-dimensional model as the simulation of plasma developing from one field emitter only.

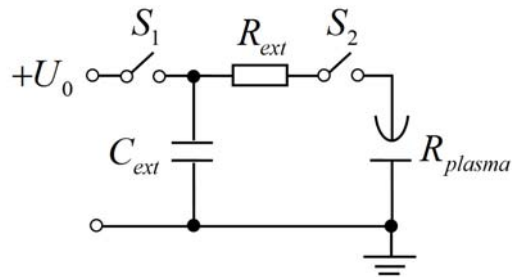
2 Methods

2.1 Experimental setup

The experimental setup to be modelled [11] consists of a rounded rod (anode) and a plane sample (cathode), with a typical gap distance of $20\ \mu\text{m}$ (Fig. 1(a)). As the high electric field is concentrated to a small area on both the anode and the cathode, the system can be approximated by two parallel plane electrodes, with a homogeneous external electric field in-between. Two modes of measurement are possible with this setup, one for measuring the electron field emission current as a function of applied field and the other for determining the breakdown field E_{BRD} . From the former, one can extract the so-called field enhancement factor β by fitting the Fowler-Nordheim equation [12, 13]. Details of the field emission model are discussed in Sec. 2.3.4. β describes by what factor the external field is enhanced at the surface. Typical measured values of the breakdown field are around $150 - 250\ \text{MV/m}$, and field enhancement factors between $40 - 70$ for copper. The corresponding local field (calculated as the product of E_{BRD} and β measured prior to breakdown) for conditioned copper was found to be more or less constant around a value $E_{LOC} \sim 10 - 11\ \text{GV/m}$ [14, 15].



(a) Experimental setup: anode (cylindrical, on the right) and cathode (planar, on the left) with a gap distance of $\approx 20\ \mu\text{m}$ in-between.



(b) Electric circuit during breakdown measurements, where $R_{ext} = 30\ \Omega$, $C_{ext} = 0.1 - 27.5\ \text{nF}$. First C_{ext} is charged, with S_1 closed and S_2 open. Then the power supply is disconnected (S_1 open) and finally the charged capacitor is connected to the discharge gap (S_2 closed).

Fig. 1 Experimental setup (a) and its schematic electric circuit during breakdown measurements (b).

To measure the breakdown field, first a capacitor is charged to a given high voltage, then it is disconnected from the power supply and finally connected to the electrodes, so that the circuit during breakdown consists of a capacitor C_{ext} (serving as a power supply), a resistor R_{ext} (limiting the current) and the discharge gap characterised by the resistance of the plasma $R_{plasma}(t)$ (Fig. 1(b)). The voltage over the electrodes is constant until breakdown starts and then falls exponentially (Fig. 2) with a given time constant depending on C_{ext} (R_{ext} is always the same). The maximum energy available for the breakdown is thus determined by the capacitance and the charging voltage.

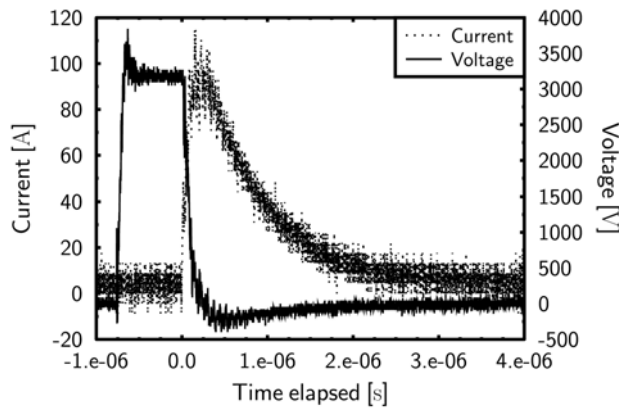


Fig. 2 Typical experimental curves for current and voltage measured over the cathode-anode system. First an external capacitor is charged to a high voltage, then this capacitor is connected to the copper electrodes. The voltage remains stable for a while, until breakdown starts and drops then exponentially. Meanwhile the current grows until the energy available for breakdown is consumed.

In a vacuum arc, experimentally measured plasma densities are typically $10^{20} - 10^{22} \text{ 1/cm}^3$ [16, 17, 18]. Total current densities are estimated to be in the regime of at least $10^{-2} - 10^{-1} \text{ A}/\mu\text{m}^2$ [19] with values up to $\sim 1 \text{ A}/\mu\text{m}^2$ [17]. In a fully developed arc, highly ionised species can be present (for copper up to Cu^{5+} [16]). In the given geometry of the experimental setup one can assume that an order of 10 field emitters are present at the same time at the breakdown site, one being the dominating field emitter [20].

2.2 The model and its applicability

An existing one-dimensional, 1d3v, electrostatic particle-in-cell code with Monte Carlo collision scheme (PIC-MCC) [21, 22, 23] has been adapted to the experimental setup described above and the relevant physical phenomena (Sec. 2.3) in vacuum arcs. In the current model, the material under investigation is copper, which is the main candidate material for CLIC accelerating structures. Two “infinite” electrodes are simulated, with the cathode grounded and the anode powered with 5 kV. The distance between the electrodes is set to $20 \mu\text{m}$, resulting in an electric field of 250 MV/m. Particles can move in one dimension along the electric field. Through collisions, their velocities are resolved in three dimensions. A schematic view of the model is given in Fig. 3.

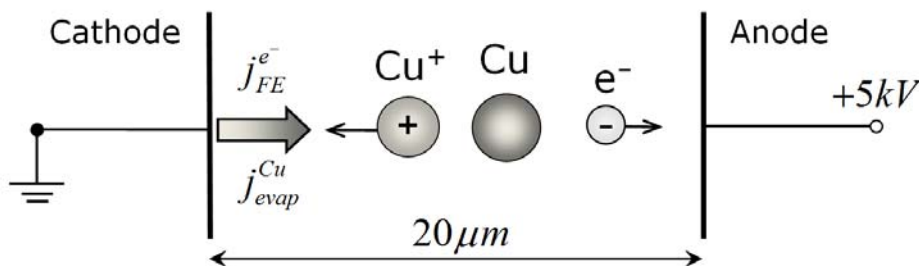


Fig. 3 Schematic diagram of the one-dimensional PIC-MCC code used for modelling DC arcs. The high electric field causes electron field emission and evaporation of neutrals. Ions are created in ionisation collisions. Three species (electrons, neutrals and ions) are taken into account.

Simulations are initiated starting from perfect vacuum, i.e. no particle at all being present in the system. In this model, only the three dominating species, electrons, Cu neutrals and Cu^+ ions, are taken into account. Electrons appear in the system due to electron field emission (Sec. 2.3.1) from a field emitter tip. This field emitter tip is assumed to be present at the cathode in terms of its field enhancement factor β , however, geometrically the emitter can not be resolved in a one-dimensional model. Neutrals appear initially due to a mixture of field and thermal evaporation to which we apply a simple model (Sec. 2.3.2) in our simulations. Throughout all the simulation, only electrons and neutrals are injected, which is a simplification mainly motivated by the fact that only Cu^+

is taken into account and no higher ionisation states. Therefore, all ions present in the system are produced in collisions (Sec. 2.3.3). Once charged particles are present in the system, they are accelerated in the electric field and can cause sputtering from the electrodes. The sputtering (Sec. 2.3.4) determines the boundary conditions and sputtered particles become the source of further neutrals and electrons. Neutrals evaporated and sputtered from the field emitter tip will erode the tip, and a high electron current density caused by emitted electrons will heat and eventually melt the tip (Sec. 2.3.5). The "melting" of the tip is performed simply by setting $\beta = 1$. Both the erosion and the melting of the tip can be taken into account in the model by assigning an area to the tip.

In principle, simulations are then terminated when the initially chosen number of time steps is finished, and simulations can be continued later on. In practice, however, simulations have to be stopped in the early stage of arc development, due to memory limitations (discussed in detail at the end of this Section).

To mimic the experimental circuit and its limited energy available for breakdown, the external voltage applied to the anode stays constant only until the current density through the electrodes reaches a certain threshold. This threshold was assigned to indicate that plasma starts to build-up and extract energy from the system. Values around $2 - 3 \cdot 10^{-3} \text{ A}/\mu\text{m}^2$ were found to be suitable for this purpose, because they correspond to the build-up of an ion current in addition to the electron current. (The choice of the threshold can slightly influence the timescale of plasma build-up.) After the threshold in current density is reached, the voltage is reduced exponentially. The time constant of this exponential drop is one of the parameters to be investigated (Sec. 3.2). In principle, the time constant $\tau = C_{ext}(R_{ext} + R_{plasma})$. However, the resistance of the plasma can not yet be calculated self-consistently because only the current density is known and the area of current flow is clearly not resolved in a one-dimensional model.

As the model is one-dimensional, several free parameters in the model remain, which will be discussed extensively in Sec. 3. These free input parameters and their implementations in the code are the following:

- i. the electron field emission current density that melts the tip (Sec. 3.1), implemented as a threshold of electron field emission current density j_{melt} , which, if exceeded, sets the field enhancement factor of the tip $\beta = 1$;
- ii. the time constant of the exponential drop in the external voltage τ (Sec. 3.2), which determines the potential at the electrodes at any instant;
- iii. the evaporation of neutrals to electron field emission ratio $r_{Cu/e}$ (Sec. 3.3), which determines how many neutrals are injected at the cathode in comparison to the electrons that are injected according to the Fowler-Nordheim equation (Eq. 1);
- iv. the initial local field E_{LOC} that acts at the field emitter tip when starting the simulation (Sec. 3.4), given by the product of the initial field enhancement factor of the tip and the initial external electric field.

These parameters together with simulation-related parameters such as time step and grid size serve as the only input parameters in the model. The development of the system is then fully determined by the model described. Within regular time steps, relevant macroscopic plasma parameters that are calculated from particle coordinates (1d) and velocities (3v) (number density of each species, potential and temperature) are outputted, as well as energy distributions at several positions in the system. Also the evolution of free parameters that vary with time (local field, field enhancement factor, exponentially dropping external potential), and the evolution of injected and absorbed particle currents at the boundaries is followed. With the aid of these, the total current density going through the discharge gap as well as the plasma resistance can be determined as a function of time.

When using a PIC code, following conditions between simulation time step Δt and plasma frequency ω_{pe} as well as grid size Δx and Debye length λ_D have to be fulfilled in order to guarantee a stable and reliable solution [22]: $\Delta t \leq 0.2\omega_{pe}^{-1}$ and $\Delta x \lesssim \lambda_D$ (we chose $\Delta t = 0.2\omega_{pe}^{-1}$ and $\Delta x = 0.5\lambda_D$). The dynamic range for resolving plasma density with pseudo-particles is limited due to memory and runtime limits to about 6 orders of magnitude. These limits can be estimated as follows. Knowing the timescale of the phenomenon to be simulated and given an acceptable runtime (a few weeks, for instance), the smallest resolvable time step can be determined. Similarly, knowing the typical densities (number of particles in a cell) in the phenomenon and given the memory available in the simulation determines the grid size that can be resolved. This means, that for a given system with given timescale and spatial size, we may choose the number of superparticles (N_{sp}) such that runtime and memory requirements are optimised, however, this determines the density around which the solution is stable.

Given the fixed dimensions of the modelled system, the practical limit of plasma density producing reliable results is $10^{19} - 10^{20} \text{ 1/cm}^3$ at a maximum, keeping the number of cells below ~ 1000 .

Specifically for arc plasma, the difficulty is that many orders of magnitude in density would have to be covered, but with one set of parameters (Δx , Δt , N_{sp}) this is not possible. One may of course stop a simulation when a given density is reached and choose different parameters so that the range of densities that can be simulated would be extended. However, due to the enormous rise of density in the arc during the ‘‘avalanche’’ of ionisation, enhancement factors in the grid size of several orders of magnitude and similar reduction factors of the time step would be needed to describe the complete phenomenon. Therefore, with PIC one is limited to the early stage of arc burning.

2.3 Phenomena taken into account

Particular attention is paid to the physical phenomena specifically important in the studied situation. The way of their implementation with respect to the plasma-surface interaction, build-up of plasma and sheath potential is presented in detail in the subsections below.

The diagnosis of the plasma sheath is carried out as follows. As in our simulations the sheath at the cathode is driven by the applied voltage, and is also influenced by the secondary electron emission, it is improper to define the sheath edge using the classical Bohm criterion. Therefore, we determine the sheath edge at the cathode qualitatively at the point where the electric field abruptly changes.

2.3.1 Electron field emission

The standard Fowler-Nordheim equation taking into account the field enhancement factor β has been used to calculate the field emission (FE) current of electrons j_{FE} [24, 25, 13]:

$$j_{FE}(E) = a_{FN} \frac{(eE_{LOC})^2}{\phi t(y)^2} \exp\left(-b_{FN} \frac{\phi^{3/2} v(y)}{eE_{LOC}}\right), \quad (1)$$

where ϕ is the work function, e the elementary charge and the local field is $E_{LOC} = \beta E$ with E being the electric field measured at the cathode. Note that in our case E is not purely the instantaneous external field applied but also contains contributions coming from the charged particles of the plasma. $t(y)$ and $v(y)$ are elliptical integral functions of the variable

$$y = \sqrt{\frac{e^3 E_{LOC}}{4\pi\epsilon_0 \phi^2}}, \quad (2)$$

where ϵ_0 is the permittivity of vacuum. The constants a_{FN} and b_{FN} stand for

$$\begin{aligned} a_{FN} &= \frac{e}{16\pi^2 \hbar} = 1.5414 \cdot 10^{-6} \frac{\text{A}}{\text{eV}}, \\ b_{FN} &= \frac{4\sqrt{2m_e}}{3\hbar} = 6.8309 \cdot 10^9 \frac{1}{\sqrt{\text{eVm}}}, \end{aligned} \quad (3)$$

when $[j_{FN}] = \text{A/m}^2$, $[E_{LOC}] = \text{V/m}$ and $[\phi] = \text{eV}$, where \hbar is the reduced Planck constant and m_e the electron mass. The Wang and Loew approximation [26] has been used for the elliptic functions $t(y)$ and $v(y)$, setting $t(y) = 1$ and $v(y) = 0.956 - 1.062y^2$. The value $\phi = 4.5 \text{ eV}$ [27] has been used as an average for polycrystalline copper.

The Fowler-Nordheim equation in the above form is no longer applicable when the electron current density reaches $\sim 0.06 \text{ A}/\mu\text{m}^2$ [10, 47], and space charge corrections become significant thereafter. Since in PIC the electric field is a sum of the external field and the fields created by charged particles, the space charge correction to the Fowler-Nordheim equation is automatically taken care of. Above an emission current of $\sim 0.06 \text{ A}/\mu\text{m}^2$, most of the emitted electrons will be absorbed again immediately by the cathode, so that the net electron emission current towards the anode will be the space charge corrected one.

In reality, part of the electron emission from the tip is thermal-assisted, however, in the model, thermionic emission [28] has not been taken into account, since the temperature of the tip is not resolved. Nevertheless,

the melting of the tip had to be incorporated into the model (discussed in detail in Sec. 2.3.5), for otherwise the electron emission current would grow unrealistically high. Due to the high electron current density flowing through the tip, the temperature of the tip is expected to grow significantly during the simulations, and near the melting point the thermionic component of the electron emission current is not negligible anymore. In fact, the lack of information on thermionic electron emission results in the underestimation of electron current right before the tip melts with up to 30% [13, 28] for the typical $E_{LOC} \sim 6 - 8$ GV/m seen in simulations. However, assigning temperature to the tip within a one-dimensional model, where areas are not resolved, would result in similar errors and is out of the scope of this model.

2.3.2 Evaporation of neutrals

Neutral atoms removed from the field emitter tip are the other species which build up the plasma. The evaporation of neutrals is the key to the question why arcs under vacuum conditions can develop at all. Therefore, the evaporation phenomenon is a crucial part of our model. Since the tip will be heated by the electron field emission current up to its melting point, the most significant contribution to the evaporation of neutrals will come from the (field assisted) thermal evaporation of neutrals from the field emitter. Until a more accurate prediction for the evaporation rate of neutrals is available, a simplified model has been applied in the present work. The evaporation rate of neutrals was assumed to follow the electron field emission current with a given ratio. This results in an exponential behaviour of the evaporation of neutrals as a function of electric field, which is also motivated by the fact that the thermal excitation of an atom is represented by the Boltzmann factor. The possible range of the evaporation of neutrals to electron field emission ratio has been investigated through simulations (Sec. 3.3).

The field evaporation [29, 30] of positive ions from the anode and possibly negative ions from the cathode, which might play a role in the early stage, has not been taken into account. Also the thermal evaporation of neutrals from outside the field emitter tip, which can play a role at elevated temperatures, was assumed to be negligible.

Both electrons and neutrals are injected into the system with Maxwellian velocity distributions, with corresponding temperatures of 0.25 eV and 250 eV for electrons and neutrals, respectively.

2.3.3 Collisions

Collisions play a central part in the code and are treated with the Monte Carlo collision scheme (MCC). As we are simulating the onset of plasma build-up, only the three dominant species, electrons, Cu neutrals and Cu^+ ions are taken into account; qualitative results are not expected to change much through handling more species. In addition, in the experimental setup only Cu^+ and Cu^{2+} have been observed with optical spectroscopy [31]. For the three species treated, following collisions are relevant and have been taken into account with experimentally measured, energy dependent cross sections [32, 33, 34]:

- Coulomb collisions between (e^-, e^-) , $(\text{Cu}^+, \text{Cu}^+)$, (e^-, Cu^+) ,
- Elastic collision $e^- + \text{Cu} \rightarrow e^- + \text{Cu}$,
- Impact ionisation $e^- + \text{Cu} \rightarrow 2e^- + \text{Cu}^+$,
- Charge exchange and momentum transfer $\text{Cu}^+ + \text{Cu} \rightarrow \text{Cu} + \text{Cu}^+$,
- Elastic collision $\text{Cu} + \text{Cu} \rightarrow \text{Cu} + \text{Cu}$.

2.3.4 Sputtering yields

Sputtering phenomena have also been built into the code. Cu and Cu^+ sputter Cu on both the cathode and the anode, with a yield depending on their impact energy. In our model, we used the empirical formula by Yamamura and Tawara [35], which is a best fit to available experimental data. In general, ions arriving at the cathode will sputter the most. After a while, when the plasma density builds up, the ion bombardment starts to be so intense at the cathode that the assumption of having single, uncorrelated bombardment events breaks down and yields obtained from low-flux experiments can no longer be applied. Above a threshold of ion flux at the cathode, the heat spike regime is reached and we apply an average enhanced sputtering yield of $Y = 1000$, based on previous molecular dynamics (MD) simulation results [36], carried out under conditions consistent with the model presented here. As a threshold of ion flux, the order of 10^{24} $1/\text{cm}^2\text{s}$ (or in terms of ion current density

$10^{-3} \text{ A}/\mu\text{m}^2$) has been used, obtained in earlier PIC simulations [36]. This suitably chosen threshold led to a smooth transition between the experimentally measured and the simulated, enhanced sputtering yield.

Ions and electrons accelerated through the plasma sheath gain kinetic energies in the keV regime under the described conditions. The high energy ions cause not only an enhanced sputtering of neutrals, but also the secondary electron yield (SEY) is significant at the cathode. Taking into account the energy dependence of the SEY is nontrivial, since experimental data is mostly available for the low ($< 1 \text{ keV}$) or the high ($> 10 \text{ keV}$) energy regime and the most important contribution in our case comes from the intermediate regime, and as a result of high-flux bombardment. However, as the primary source of electrons is field emission and not SEY, an estimated average value of $SEY = 0.5$ has been used for ion impact at the cathode, motivated by experimental upper and lower limits of $SEY = 2$ for an incident energy of 10 keV [37], and the order of $SEY \sim 0.01$ for slow ions, respectively (an estimate based on [38]). Simulations carried out with $SEY = 0.01, 0.5, 2$ and otherwise the same parameters, showed that the value of SEY influences only slightly the time it takes for the plasma to build up. Also secondary electron emission (SEE) at the anode can influence the electron dynamics. This is not expected to change the characteristics of plasma build-up much, as the mechanism has been implicitly parametrised and tested through increasing the SEY up to 2.

Note that in experiments, electron stimulated desorption (ESD) of neutral or charged molecules and atoms [39], as well as low-energy electron-induced sputtering [40], could play an important role at the anode, both mainly due to surface impurities present in the samples [41, 42]. In simulations, however, a pure material is modelled, therefore both effects were assumed to be negligible.

2.3.5 Eroding and melting the field emitter tip

The plasma obtained from one single tip is simulated with our one-dimensional model, so the erosion and finally the melting of this tip has to be included in the model. For explicit calculations in the code, a cylindrical tip with 20 nm radius has been assumed.

The erosion of the tip is simply determined by counting the number of neutral particles injected at the cathode, which is the sum of sputtering yield and evaporation. The “height” ($h \approx \beta r$ [43]) of the tip is reduced linearly with the number of neutrals injected, through the decrease of β . Simulations showed that the erosion of the tip is $\lesssim 1\%$ before the electron current melts the tip, so that the change in β due to erosion is not significant; the local field will fluctuate much more as a consequence of fluctuations in the potential.

The electron current density that melts the tip modelled, has been estimated based on a calculation solving the heat conduction equation [44], and gave the order of $1 \text{ A}/\mu\text{m}^2$. The Nottingham effect, which would give only a small correction for a cylindrical tip [45], has not been taken into account for this order of magnitude estimate. Hereinafter, by the term “melting current” (j_{melt}) a threshold of electron emission current density is understood that melts the tip. When this threshold is exceeded, β is set to 1. ($\beta = 1$ corresponds to a flat surface and a completely eroded field emitter. In reality, part of the field emitter could remain so that $\beta_0 > \beta > 1$.)

It was mentioned already, that for high field emission currents, the net electron current towards the anode will be significantly smaller than the originally emitted one. Note that the melting of the tip is attributed here to the *emitted* electron current only, since the electron current reabsorbed at the cathode will be distributed over a much larger area ($\mathcal{O}(\mu\text{m}^2)$), than the area of the field emitter tip ($\mathcal{O}(\text{nm}^2)$).

3 Results

The sequence of events, as seen from the simulations, that leads to plasma formation is the following. Starting the process of arcing in vacuum, the first two species which appear in the system are electrons and neutrals, due to the high electric field. Neutrals are then ionised by the electrons that are accelerated in the electric field. Electrons and neutrals being constantly emitted, e^- , Cu and Cu^+ densities build up accordingly. An avalanche of ionisation is reached, when the mean free path l_{mfp} of the electron impact ionisation (given by the Cu density and the experimental value of the cross section of Cu ionisation) becomes smaller than the spacing between the electrodes l_{sys} , which happens around a neutral Cu density of 10^{18} 1/cm^3 . This is the criterion for unavoidable plasma formation, since the sputtering due to the ion flux at the electrodes will create even more neutrals in the system, leading to increased ionisation, which then again results in an enhanced ion flux, in enhanced erosion

of the electrodes, and so forth. As long as energy is available, the current density of the arc rises steadily too, accompanied by the rapid reduction of electrical resistance; breakdown occurs.

We can formulate two conditions required for the plasma to build up. The first condition to be fulfilled is a *high enough initial local field*, which after stabilising first to a given value, grows then slightly, resulting in a huge electron field emission current growth, until the melting current is reached. During this period, the ion density still remains below the electron density, and so the plasma sheath is not established yet. Instead, just before the melting of the tip, the potential is usually zero in the first $\sim 2/3$ of the system seen from the cathode, indicating the screening of the external potential by electron space charge (cf. Fig. 5). When the ion density has built up sufficiently, a sheath can form, which happens around the same timescale as the melting of the tip. The second condition to be fulfilled is reaching the *critical neutral density*, or equivalently, meeting the requirement that $l_{mfp} < l_{sys}$ for the electron impact ionisation. Depending on the state of the system, two cases are possible: Either (i) the neutral density remains below critical, and charged particle densities remain then even below the neutral density and no arc plasma builds up; or (ii) the avalanche of ionisation is reached, the sheath leads to a local field at least as high as initially with $\beta > 1$, plasma is maintained and densities grow until the energy available for breakdown is consumed.

A four-dimensional parameter space has been sampled with simulations and the reaction of the plasma to the changes in initial parameters has been investigated. Setting different initial parameters can result in very different plasma behaviour and knowing the regime in which plasma build-up is facilitated and in which it is not, can suggest ways how to lower the breakdown probability. The parameters examined were: (i) the melting current, which will change with the geometry of the tip; (ii) the time constant of the external circuit, scaling the energy available for breakdown; (iii) the evaporation of neutrals to field emission current ratio, to give an estimate on the range in which it can move, and finally, (iv) the initial local field needed for ignition, a quantity that can be directly compared with experiments.

As mentioned before, E_{LOC} for copper at breakdown is always around 10 GV/m [14]. In experiments, the energy available for breakdown has been varied, and even with different amounts of energy available, E_{LOC} remained the same [31]. Consequently, this value has been assumed throughout all the simulations (except for series (iv)), using typical experimental values of an initial external electric field $E_0 = 250$ MV/m and $\beta = 40$.

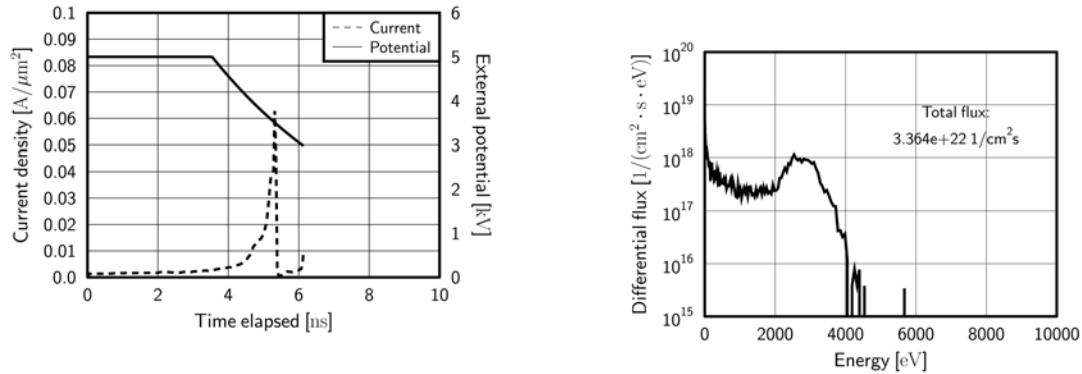
3.1 Melting current

The influence of the melting current has been examined in the region $j_{melt} = 0.4 - 1$ A/ μm^2 . Above 1 A/ μm^2 , additional information can not be gained due to limited simulatable density. Simulations have been carried out for melting currents of 0.4, 0.5, 0.6, 0.8, 0.9 and 1 A/ μm^2 , with a time constant (Sec. 3.2) of $\tau = 5$ ns and an evaporation of neutrals to electron emission current ratio (Sec. 3.3) of $r_{Cu/e} = 0.01$ for all of them. (Note that timescales are rather sensitive to the parameter $r_{Cu/e}$. This will be further discussed in detail in Sec. 3.3). The plasma was in all of these cases beyond the “point of no return”, where ionisation and the development of an arc are unavoidable. This confirmed that the estimated regime of $j_{melt} = 0.4 - 1$ A/ μm^2 provides a sufficient amount of electrons for the onset of plasma, and in combination with $r_{Cu/e} = 0.01$ and $\tau = 5$ ns initial conditions are suitable for plasma to build up. Therefore factors that can influence the melting current such as the dimensions (height, area perpendicular to j), the geometry (cylindrical, conical etc.) and the composition (oxides, impurities) of the tip, do not seem to influence arc development. (However, they may influence the triggering of the formation of field emitter tips.)

After the electron current density has reached its peak, the plasma ionises completely (neutrals are present only in the sheath region) and a sheath forms that is able to maintain itself thereafter. An example for $j_{melt} = 0.5$ A/ μm^2 is shown in Fig. 4(c). The total current (Fig. 4(a)) starts to grow once more after its first peak, that is due to the high electron emission before melting; this is the onset of arcing. At 6.13 ns the simulation exceeds its numerical limits due to high neutral density at the cathode. The Cu^+ energy distribution at the cathode (Fig. 4(b)) averaged over the onset phase (5.35 – 6.13 ns) shows a peak around 3 keV, as a consequence of a sheath potential of ~ 3 kV.

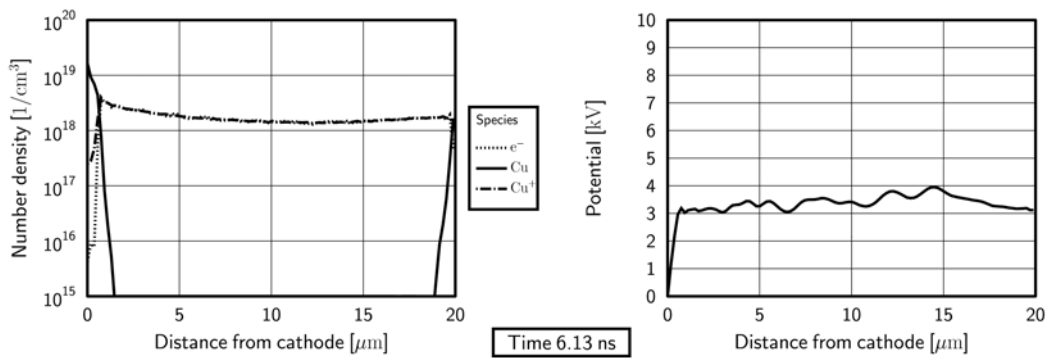
In the whole regime of $j_{melt} = 0.4 - 1$ A/ μm^2 the effect of space charge on the electron emission current can be seen in terms of the potential (Fig. 5). The higher j_{melt} , the more this effect is enhanced. Qualitatively j_{melt} does not influence plasma behaviour much, but in the region $j_{melt} = 0.8 - 1$ A/ μm^2 numerical limits restricted

the simulations to the electron emission phase. To simulate the plasma onset, it was numerically convenient to use $j_{melt} = 0.5 \text{ A}/\mu\text{m}^2$ for the investigation of all other parameters.



(a) External potential and total current through the discharge gap.

(b) Average Cu^+ energy distribution at the cathode.



(c) Density of different species (left) and electric potential (right) in the plasma

Fig. 4 Examining the influence of the melting current. The qualitative behaviour remains the same for the whole regime investigated ($j_{melt} = 0.4 - 1 \text{ A}/\mu\text{m}^2$). In the particular case shown here $\tau = 5 \text{ ns}$, $r_{Cu/e} = 0.01$ and $j_{melt} = 0.5 \text{ A}/\mu\text{m}^2$. After the first peak in the total current, a sheath has built up and the total current grows again. (Note that the total current is the sum of the ion and the space charge limited electron current, and stays therefore below j_{melt} .) Fig. (b) shows the average energy distribution of ions bombarding the cathode during the burning of the arc. The densities of different species in the plasma and the corresponding electric potential at the last instant before the simulation exceeds its numerical limits are shown in Fig. (c). Neutrals are present only in the sheath region, while outside the sheath region the plasma is quasi-neutral (electron and ion densities are the same). Quasi-neutrality outside the sheath is reflected also in the constant potential (fluctuations in the potential are due to growing numerical instability at this last instant), whereas the sheath potential originates from the difference in ion and electron densities in the sheath region. Note that also close to the anode there is a sheath potential drop present ($\sim 200 \text{ eV}$, corresponding to an electron temperature of $\sim 40 \text{ eV}$), however, it is difficult to notice it on the scale of Fig. (c).

3.2 Time constant

Possible changes in plasma properties were examined as a function of energy available. Experimentally, this was done through changing the capacitor that supplies the discharge; the energy range covered was $5 \text{ mJ} - 1.5 \text{ J}$. One observation was that both breakdown and local field (and thus also β) remain approximately the same. Therefore, different capacitors will be equivalent to different time constants and energies. The current-voltage characteristics

of the discharge remained qualitatively the same, but both the current reached and the timescale of the discharge scaled with the energy available. Corresponding time constants varied in the range 3 ns – 1 μ s. In simulation, the range 1 – 100 ns is realisable and simulations have been carried out for $\tau = 2, 3, 4, 5, 5.6, 6, 7, 10, 20$ and 100 ns, with common parameters $j_{melt} = 0.5 \text{ A}/\mu\text{m}^2$ and $r_{Cu/e} = 0.01$.

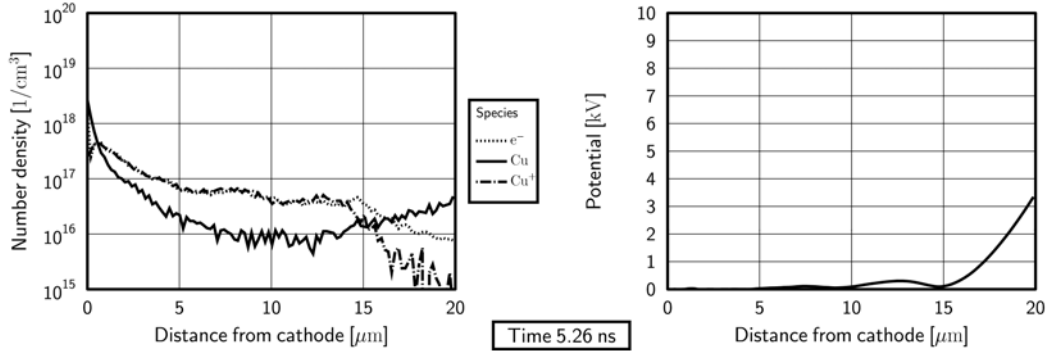
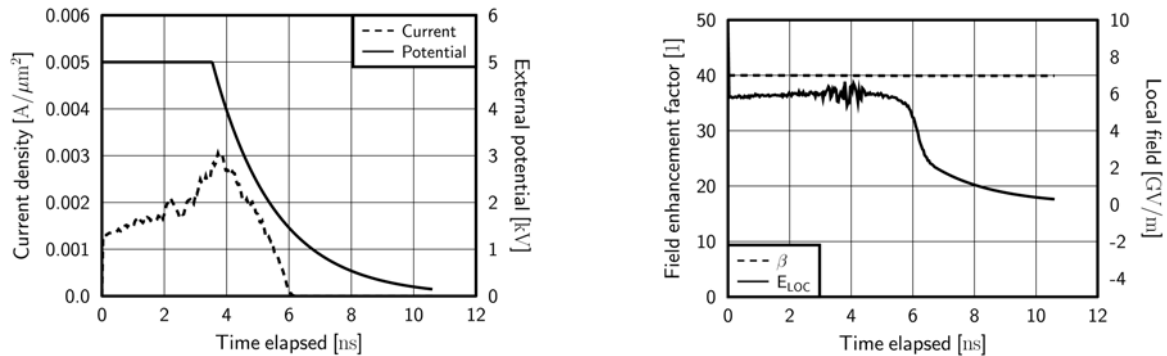


Fig. 5 The effect of space charge during high electron emission current. Before the formation of the sheath, as long as the ion density is still smaller than the electron density, the potential is screened in about 2/3 of the system starting from the cathode where electrons are emitted. Simulation parameters were $\tau = 5$ ns, $r_{Cu/e} = 0.01$ and $j_{melt} = 0.9 \text{ A}/\mu\text{m}^2$.

An important prediction of this series was that below a given time constant, no breakdowns would occur. Practically no plasma builds up at all, as in the case of $\tau = 2$ ns (Fig. 6). Intuitively, such a threshold should exist, below which there is simply no time to create a plasma starting from vacuum. Nevertheless, no exact value for this threshold can be given with our model, since the timescale is highly influenced by $r_{Cu/e}$ (cf. Sec. 3.3). In DC experiments, this threshold has not been reached yet and it does not seem to be feasible to lower the time constant further. However, RF structure testing experiments show indications of such a threshold: Travelling wave structures tested with 3 – 5 ns pulses could attain a surface field twice as high as usual ($\sim 600 \text{ MV/m}$) [46].



(a) External potential and total current through the discharge gap

(b) Evolution of β and the local field at the cathode

Fig. 6 A simulation with a time constant of $\tau = 2$ ns. No breakdown is occurring, implying that the plasma needs — with the given initial conditions ($j_{melt} = 0.5 \text{ A}/\mu\text{m}^2$, $r_{Cu/e} = 0.01$) — at least ~ 4 ns in total to build up. The timescale is sensitive to $r_{Cu/e}$. Also the threshold, at which the voltage starts to drop exponentially, is only estimated and can modify slightly the timescales.

For $\tau \geq 3$ ns, breakdown does occur, but with two different regimes depending on τ . Below 10 ns, the neutral density is very close to the critical density and small changes in the initial conditions can influence whether the ionisation avalanche can be reached or not. For $\tau = 3, 4, 5$ and 6 ns, the plasma sheath was sustained until all the neutrals in the system, except for those in the sheath region, were ionised, while for $\tau = 5.6$ and 7 ns ionisation could not be reached. Although in reality many other factors will influence the timescale of plasma build-up (E_{LOC} , $r_{Cu/e}$ etc.) and such a closeness to the critical density might not be observed, it is interesting to examine what causes this effect. In the case of $\tau = 5.6$ and 7 ns, the sheath remains sustained once it is created, nevertheless, not all the neutrals can be ionised. This is due to the fact that the neutral density fulfils the criterion for an ionisation avalanche only close to the cathode and only temporarily, then it drops below the critical density. As a consequence, Cu density is higher than e^- or Cu^+ density, both of which remain below 10^{18} $1/cm^3$. This relatively “low-density” plasma populated mostly by neutrals does not show the characteristics of an arc plasma (such as an ionisation avalanche, growing current density, a high flux of high energy ions bombarding the cathode, etc.). Above 10 ns, the ionisation process takes place unavoidably in all of the cases, and an arc plasma forms.

Also the timescale of plasma build-up changes slightly with τ . Between $\tau = 3 - 5$ ns, a double peak could be seen in the total current, with the first peak corresponding to the electron emission phase and the second peak corresponding to the build-up of plasma (cf. Fig. 4(a)). This second peak occurred while $\beta = 1$ and, due to the sheath, $E_{LOC} \sim 7 - 8$ GV/m. Above 5 ns, the second peak overlaps with the first one, the rise in current density due to plasma build-up can barely be distinguished from the rise due to electron emission (cf. Fig. 11(b)).

The statistics of highest current density and local field reached after the melting of the tip for $\tau = 3 - 100$ ns can be seen in Fig. 7, showing the proximity to the critical density below $\tau = 10$ ns in terms of E_{LOC} . All ion energy distributions at the cathode extracted for $\tau = 4, 6$ and 20 ns gave a peak around 3 keV and a total flux of $\sim 5 \cdot 10^{22}$ $1/(cm^2s)$. In comparison, the ion energy distribution for $\tau = 7$ ns, where not all the neutrals could be ionised, gave also a peak around 3 keV, but a much narrower one. In addition, the flux reached only $\sim 3 \cdot 10^{21}$ $1/(cm^2s)$ directly after the melting of the tip, and contrary to the fully ionised case, then started dropping. Simulations $\tau = 4, 6$ and 20 ns were also repeated with $j_{melt} = 0.9$ $A/\mu m^2$, but they all exceeded numerical limits: Memory limitations caused simulations to break down almost immediately after ionisation has started due to a quick rise in density.

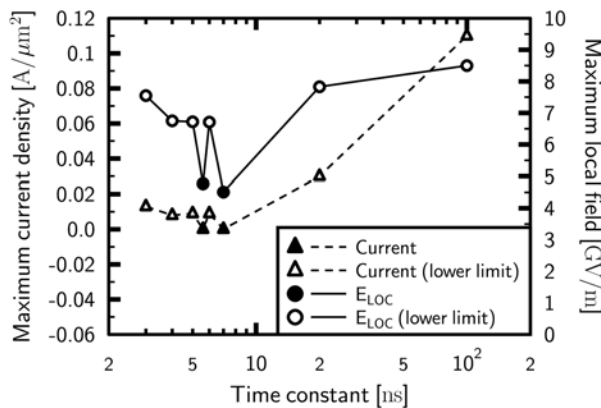


Fig. 7 Statistics for the highest current density and local field reached in each simulation after the melting of the tip, as a function of τ . Below 10 ns, the neutral density is close to critical. E_{LOC} reflects whether an arc can develop or not. For $\tau = 5.6$ and 7 ns, only a relatively low-density plasma can build up (densities stay below $\sim 10^{18}$ $1/cm^3$). Above 10 ns, an arc plasma develops unavoidably. Only lower limits can be presented for those cases in which an arc develops, since simulations are restricted to the onset phase.

3.3 Evaporation of neutrals to electron field emission ratio

Although $r_{Cu/e} = r_{Cu/e}(E, t, \dots)$ is treated in our simple model of evaporation of neutrals as a constant, it is valuable to have a theoretical estimate in which regime it can move. Simulations covered $r_{Cu/e} = 0.001, 0.005, 0.008, 0.01, 0.025, 0.05$ and 0.1 for both $\tau = 4$ ns and $\tau = 20$ ns, with $j_{melt} = 0.5$ $A/\mu m^2$.

The rate of neutrals compared to electrons in the system will influence how quickly different processes will take place; e.g. it can either enhance or slow down ionisation. For $r_{Cu/e} = 0.001 - 0.008$, most of the neutrals can not be ionised ($n_{Cu} > n_{Cu^+}, n_{e^-}$) and all densities stay rather low so that the ionisation avalanche can not be reached. Also the local field created by the sheath of this “low-density” plasma is rather small ($\sim 2 - 3$ GV/m

at maximum). In contrast, already for $r_{Cu/e} = 0.01$ all neutrals get ionised and also the sheath results in significantly higher fields (~ 7 GV/m). Above $r_{Cu/e} = 0.01$, the higher $r_{Cu/e}$ is, the stronger also the effect of potential screening.

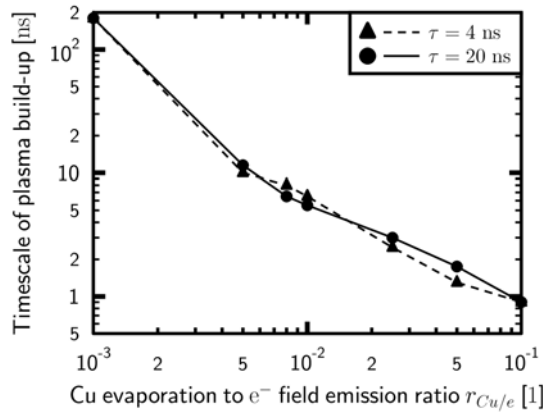


Fig. 8 Influence of the evaporation of neutrals to electron field emission ratio on the timescale of plasma build-up. The timescale is defined here as the time needed for the first peak in total current density to occur, which corresponds to high field emission prior to plasma build-up. For the lowest ratio, $r_{Cu/e} = 0.001$, the value presented is only an upper limit. The time constant used in the simulation does not influence these timescales significantly, only about 10%.

The time needed for the (first) peak in total current density to occur, is summarised for all the cases in Fig. 8, which shows how the time needed for plasma build-up scales with $r_{Cu/e}$. Comparing theoretical and experimental timescales, the evaporation of neutrals can be estimated to be in the regime $r_{Cu/e} \sim 0.01 - 0.05$. Even though DC and RF can not be easily compared, very fast plasma build-up can be excluded since otherwise it would be in contradiction with the fact that short pulses are not likely to produce breakdowns in RF (in RF experiments, most of the breakdowns occurred between 8 – 60 ns after the peak field [4]). Very slow build-up can be excluded too, since low values of $r_{Cu/e}$ do not produce an arc plasma with high densities.

3.4 Initial local field

Up to now, an initial $E_{LOC}^0 = 10$ GV/m has been assumed, based on experimental results. A final issue to examine is, how sensitive plasma build-up is to E_{LOC}^0 , the initial electric field E_0 and the initial β . Altering β and E_0 without altering E_{LOC}^0 did not result in a different behaviour of the plasma (conclusion from simulations with $\beta = 30$, $E_0 = 333$ MV/m and $\beta = 50$, $E_0 = 200$ MV/m instead of the usual $\beta = 40$, $E_0 = 250$ MV/m; common parameters were $j_{melt} = 0.5$ A/ μm^2 , $\tau = 4$ ns and $r_{Cu/e} = 0.01$). The typical time evolution of E_{LOC} is presented in Fig. 9. Even though starting from $E_{LOC}^0 = 10$ GV/m, E_{LOC} soon stabilises to a value typically ~ 6 GV/m, slightly growing before breakdown. With growing electron emission, E_{LOC} becomes more and more unstable. After the melting of the tip, in case a sheath forms, E_{LOC} can reach values around 6 – 8 GV/m, depending on initial conditions.

Lowering E_{LOC}^0 through either lowering β or lowering E_0 resulted in drastic changes in the current density. With initial conditions $\beta = 40$ and $E_0 = 200$ MV/m (i.e. $E_{LOC}^0 = 8$ GV/m), the electron FE current can still melt the tip but the ionisation avalanche is not reached anymore. For conditions $\beta = 30$, $E_0 = 250$ MV/m ($E_{LOC}^0 = 7.5$ GV/m) and $\beta = 40$, $E_0 = 150$ MV/m ($E_{LOC}^0 = 6$ GV/m), no plasma evolved at all. Comparing to Fig. 9 and seeing that the initial field drops down to 6 GV/m almost immediately, one might ask why there is no plasma forming for $E_{LOC}^0 = 6 - 8$ GV/m. The key to this is the fact that for $E_{LOC}^0 = 6$ GV/m the local field stabilises around 4 GV/m, for $E_{LOC}^0 = 7.5$ GV/m around 5.5 GV/m and for $E_{LOC}^0 = 8$ GV/m slightly below 6 GV/m, so that the condition for plasma to build up appears to be stabilising the local field at least up to 6 GV/m to reach a sufficiently high electron field emission current.

For copper, $E_{LOC}^0 = 10$ GV/m corresponds already to an experimentally measured breakdown rate $BDR = 1$, meaning that the probability of a breakdown occurring when applying this field is 1. One might ask then what happens for $E_{LOC}^0 > 10$ GV/m. Interestingly, the initial conditions $\beta = 30$, $E_0 = 300$ MV/m and $\beta = 48$, $E_0 = 250$ MV/m, both corresponding to $E_{LOC}^0 = 12$ GV/m, showed a stabilisation of the local field again around 6 GV/m, and not higher. This means that even for $E_{LOC}^0 > 10$ GV/m the FE current will regulate itself down to the same level as for $E_{LOC}^0 = 10$ GV/m.

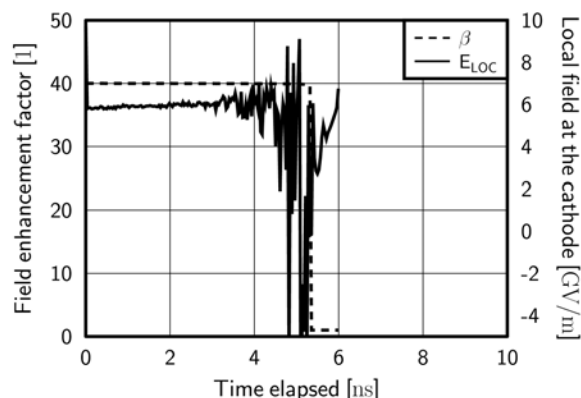


Fig. 9 Typical time evolution curve of β and the local field when starting from an initial $E_{LOC}^0 = 10$ GV/m. Before breakdown, E_{LOC} typically falls down to ~ 6 GV/m and then grows slightly. The fluctuations correspond to the period where electron emission is enhanced significantly. After the tip is molten, the local field drops accordingly. In case a plasma sheath can form and maintain itself, E_{LOC} can reach afterwards values up to 6 – 8 GV/m during the plasma build-up phase.

The fact that the efficiency of plasma development drops drastically for $E_{LOC} < 10$ GV/m confirms that, for plasma build-up from a field emitter tip, $E_{LOC} = 10$ GV/m is required within its experimental error of $\pm 16\%$ [15]. However, the initial $E_{LOC} = 10$ GV/m might rather set a condition to the formation of field emitter tips during the onset phase of arcing, than to the build-up of plasma, which requires only $E_{LOC} \sim 6$ GV/m to produce a growing field emission current. An indication for this might also be the fact that the experimentally measured $E_{LOC} = 10$ GV/m required for copper to break down is the value for *conditioned*¹ copper, where tips have to be formed first before breakdown. For non-conditioned copper, E_{LOC} can be significantly lower.

4 Discussion

A diagram summarising the simulated parameter space and its main characteristics is given in Fig. 10.

Clearly, a one-dimensional model has free parameters that can be eliminated in a two-dimensional model: For instance, j_{melt} could be eliminated in a two-dimensional model where areas are resolved and therefore temperature can be assigned to the field emitter tip. Also the drop of the external potential could be self-consistently implemented and no assumption of a time constant τ would be needed. Due to these free parameters, the results of the presented one-dimensional model should be interpreted on a qualitative level. To what extent experiments and simulations can be compared is discussed below.

The model that has been presented describes plasma build-up under breakdown conditions from only a single field emitter tip. When comparing with experimental results, it has to be taken into account that the total arc plasma will be a spatial and temporal overlap of multiple tips. Plasma igniting at one site results in intense ion bombardment at the cathode and clusters flying out of the cathode spot can ignite the plasma at another site. Thus the plasma observed in experiments could be interpreted to consist of several “generations” of plasma originating from field emitter tips, where in each such “generation”, several tips (~ 10 field emitters in the DC setup, one dominating) would be present at the same time.

The implications of the results obtained in Sec. 3 have to be discussed in the light of this tip-overlap-model. The characteristics of model and experiment can almost directly be compared (Fig. 11(a) and 11(b)), the only missing factor is the area of current flow, which is a dynamic quantity. The quick rise in current during the build-up of plasma seen in experiments is reproduced also in simulation and reflects a characteristic feature of arcs, namely that they can short-circuit even vacuum within a short time ($\sim 10 - 100$ ns). However, looking at the experimental curve, one should note that the maximum current drawn by the arc will depend on how long the arc can be sustained (how many arc spots are involved in the process). In simulations, two phenomena can contribute to high current density values: (i) a peak in electron field emission and (ii) an established arc plasma. Sometimes

¹ By a conditioned material, we mean a material, that has suffered already some breakdowns, and consequently, has an eroded surface layer. Both in RF and DC experiments, materials exhibit a “conditioning”, which means that their breakdown field stabilises after a few sparks to a value which is either higher or lower than initially. Experiments suggest that conditioning might be due to the removal of oxide from the surface.

these peaks corresponding to (i) and (ii) are separate, sometimes they grow together, depending on the timescale of (i) compared to when the avalanche of ionisation is reached. Nevertheless, in experiments (i) can not be seen, since FE occurs on a much smaller area and has therefore a minor contribution to the total current.

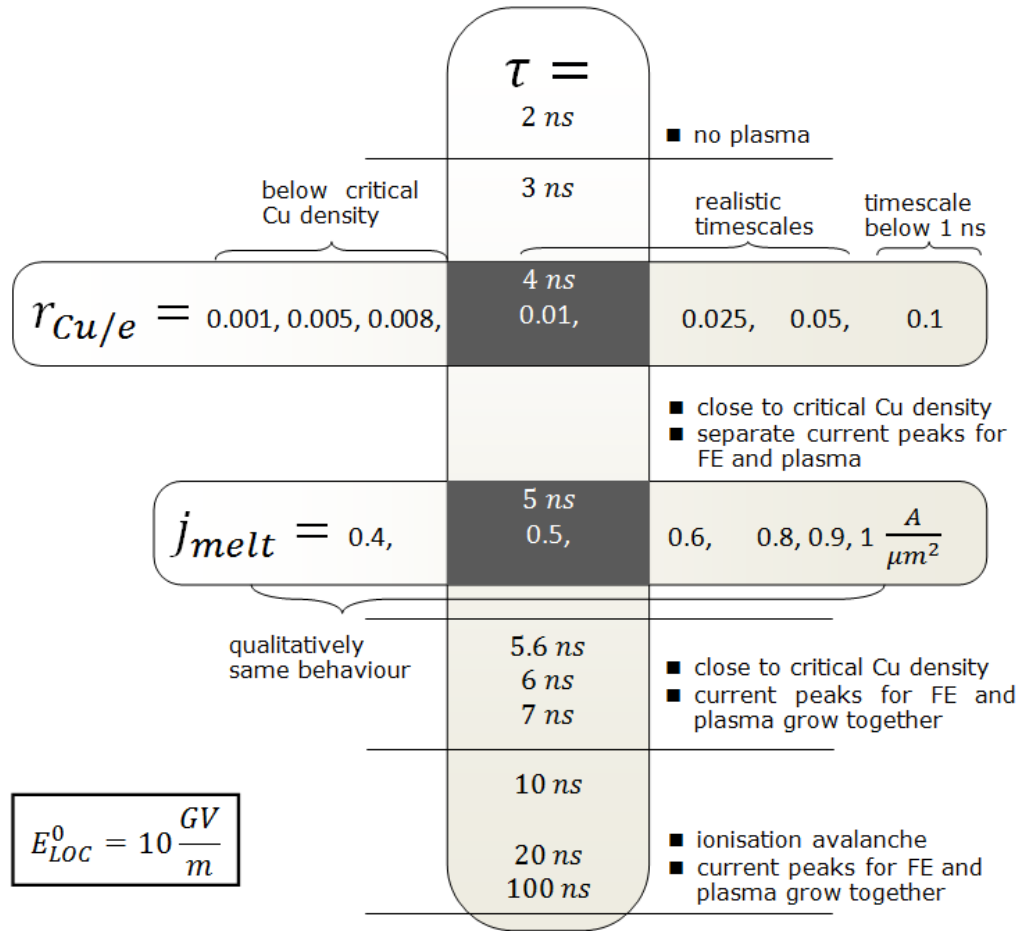
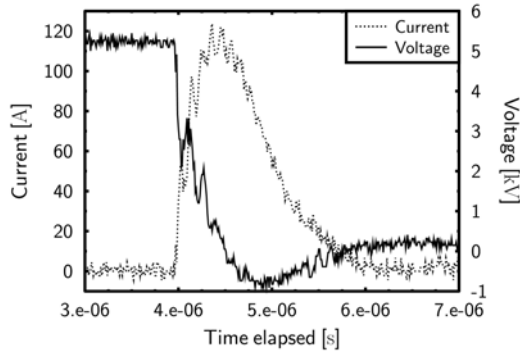


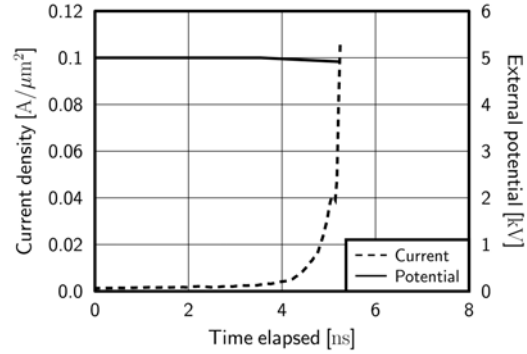
Fig. 10 Summary of the parameter space simulated. In all of the cases, $E_{LOC}^0 = 10 \text{ GV/m}$. Different simulation series can be seen in the rounded boxes. Common parameters used during a given series are indicated by the dark areas. Comments on main characteristics in a given region are also given.

The scaling of the maximum total current and the timescale of reaching this maximum with the time constant (or equivalently, with the energy available) was experimentally measured. Shorter time constants result in shorter burning of the arc, with less current, so that the total energy consumed by the arc is directly proportional to τ . This observation can not directly be compared to simulation, since for long time constants, plasma jets that are ejected from the arc spots could ignite new spots as it is known from experiments [3], [16] and was confirmed by former simulations [36], so that a different amount of “generations” would be present for low-energy arcs than for high-energy arcs.

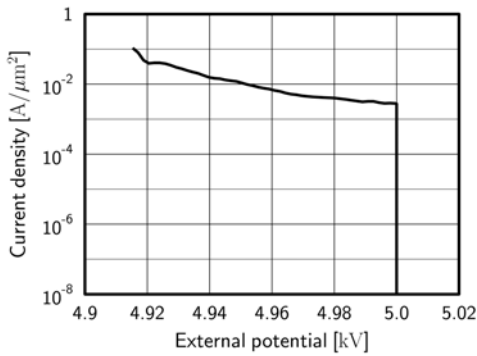
This idea is also motivated by comparing the energy consumption of simulated and experimental arcs. In simulation, the energy density consumed by the arc plasma was always between $0.5 - 1 \cdot 10^{-5} \text{ J}/\mu\text{m}^2$, regardless of initial conditions. Assuming an average ion bombardment area of $\sim 100 \mu\text{m}^2$ (based on the size of molten spots in scanning electron microscope images), we get $0.5 - 1 \text{ mJ}$ for the energy consumed by the plasma of one field emitter tip. Thus for the lowest energy experiments with 5 mJ , at maximum $5 - 10$ tips could be coexisting (even more, if the β of one tip dominates). In comparison, for experimental discharges of 1.5 J , the ignition of several subsequent arc spots would be possible, while the ions and electrons from the initial spots are already present in the system; the discharge maintains itself longer and higher total current can be drawn.



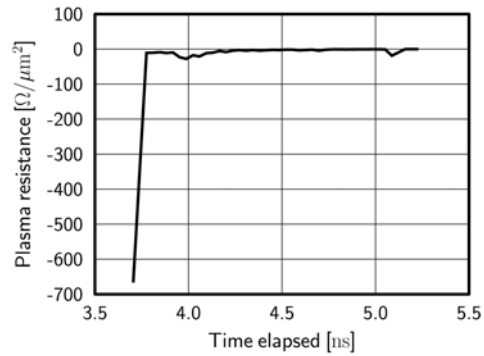
(a) Characteristic experimental curves, $\tau \approx 200$ ns with $C_{ext} = 15$ nF. The negative values after the sudden drop in voltage are purely instrumental. The measurement of shorter timescales is difficult due to growing noise, impedance of cables etc.



(b) Characteristic simulated curves, $\tau = 100$ ns. Simulations are limited to the build-up phase of the plasma. Assuming a bombardment area of $100 \mu\text{m}^2$, the simulated current density would correspond to a current up to 10 A.



(c) Simulated voltage-current characteristics corresponding to Fig. 11(b). In the beginning, the discharge gap results in an open circuit, only a small leakage current flows through it that does nearly not affect the voltage. As the plasma forms, the discharge gap gets conducting. (Note: The time evolution in the plot is from the right to the left.)



(d) Simulated plasma resistance corresponding to Fig. 11(c), after the voltage starts dropping. The plasma resistance is negative and drops quickly during its formation orders of magnitudes.

Fig. 11 Comparison of the modelled (b-d) and experimentally measured (a) development of current and voltage over the discharge gap as a function of time. In terms of total current, the characteristic behaviour of the plasma seen in experiments is reproduced by the model, the only missing factor is the area of current flow, which is also a function of time.

Finally, we would like to mention some interesting properties of the plasma as a part of an electric circuit. The plasma has negative resistance (i.e. growing driven current for dropping voltage), as can be easily concluded from Fig. 11(a). Also in simulations, this characteristics is reproduced (Fig. 11(b), 11(c) and 11(d)). When analysing experimental data of the exponential drop of the voltage, the time constant obtained will be $\tau = R_{TOT}C_{ext}$, where C_{ext} is the capacitance of the external capacitor (assuming other capacitances in the system are negligible) and R_{TOT} will be the sum of the external resistance R_{ext} and the resistance of the plasma R_{plasma} . From experiments it turns out that $R_{TOT} \ll R_{ext}$ [31], suggesting that the plasma will match the impedance of the external circuit as much as possible in order to extract energy in the most efficient way. In the ideal case, when

$R_{plasma} = -R_{ext}$, half of the available energy can be consumed by the plasma, giving an upper bound for what energy can actually be transferred to the plasma.

5 Conclusions and outlook

A one-dimensional particle-in-cell model has been developed to describe the build-up of plasma in electrical arcs and sparks resulting from a single field emitter tip. A better understanding of the sequence of the phenomena leading to the build-up of plasma in vacuum arcs has been achieved: The two key criteria to be fulfilled for a breakdown to occur are a high enough initial local field to produce a sufficient amount of electrons and a high enough neutral density to meet the criterion $l_{m,fp} < l_{sys}$ leading to an avalanche of ionisation.

A four-dimensional parameter space has been analysed for copper and parameters leading to plasma build-up have been identified. A local field of at least 10 GV/m is necessary for ignition and evaporation of neutrals to electron field emission ratios $r_{Cu/e}$ between 0.01 – 0.05 match experimentally observed timescales. With the aid of the model, one could also estimate ~ 5 ns as a minimum timescale for the plasma to build-up. The melting current, and therefore the geometry of the tip, does not influence the onset of arcing from the plasma formation point of view.

The one-dimensional model presented allows also for a qualitative comparison to experiments concerning the circuit characteristics of the plasma, the energy consumed by the plasma, the timescale of plasma build-up etc. It can give an order of magnitude estimate of the conditions ruling in the build-up phase of the discharge such as the densities, temperatures and energy distributions of each species, and the overall potential. Furthermore, the fact that both qualitative results as well as quantitative estimates of the simulation model give reasonable agreement with experimental results indicates that the theory of having field emitter initiated arcing is able to explain experimental findings and therefore to give an estimate of the number and generations of field emitters present during an arc.

Further extension of the work to a two-dimensional model is currently under development. This will allow a fully self-consistent coupling between PIC and MD simulation of surface modification, as well as between the external circuit and the discharge gap, because then also the area and the radial flux distribution of the arc will be known. In addition, further physics refinement will be done by including thermionic emission, SEE and the generalisation from DC to RF. The current model with its estimates on evaporation rates of neutrals serves furthermore as a good basis for future work towards a refined neutral evaporation model, where direct field evaporation of neutrals is also taken into account.

References

- [1] G. McCracken, J. Nucl. Mater. **93-94**, 3-16 (1980).
- [2] D. Raboso, Multipactor breakdown: Present status and where are we heading (2008), At the 6th international workshop on Multipactor, Corona and Passive Intermodulation (MULCOPIM 08), Valencia, Spain.
- [3] R. Behrisch, Surface erosion by electrical arcs, in: Physics of Plasma-Wall Interactions in Controlled Fusion, edited by D. E. Post and R. Behrisch, NATO ASI Series, Series B: Physics Vol. 131 (Plenum Press, New York, 1986), pp. 495-513.
- [4] H.H. Braun, S. Döbert, I. Wilson, and W. Wuensch, Phys. Rev. Lett. **90**(22), 224801 (2003).
- [5] M. Kildemo, Nucl. Instrum. Methods Phys. Res., Sect. A **530**(3), 596–606 (2004).
- [6] M. Kildemo, S. Calatroni, and M. Taborelli, Phys. Rev. ST Accel. Beams **7**(9), 092003 (2004).
- [7] S. Jun and L. Guozhi, IEEE Trans. Plasma Sci. **33**(October), 1487-1490 (2005).
- [8] P. Rossetti, F. Paganucci, and M. Andrenucci, IEEE Trans. Plasma Sci. **30**(4), 1561-1567 (2002).
- [9] G. Mesyats and D. Proskurovsky, Pulsed Electrical Discharge in Vacuum (Springer-Verlag, Berlin, 1989).
- [10] R. Latham (ed.), High Voltage Vacuum Insulation Basic Concepts and Technological Practice (Academic Press, London, 1995).
- [11] A. Descoedres, T. Ramsvik, S. Calatroni, M. Taborelli, and W. Wuensch, Phys. Rev. ST Accel. Beams **12**(3), 032001 (2009).
- [12] R.H. Fowler and L. Nordheim, Royal Society of London Proceedings Series A **119** (May), 173-181 (1928).
- [13] K.L. Jensen, Y.Y. Lau, D.W. Feldman, and P.G. OShea, Phys. Rev. ST Accel. Beams **11**(8), 081001 (2008).
- [14] M. Taborelli, S. Calatroni, and M. Kildemo, Breakdown resistance of refractory metals compared to copper, in: Proceedings of EPAC 2004, Lucerne, Switzerland, (2004).
- [15] A. Descoedres, Y. Levinsen, S. Calatroni, M. Taborelli, and W. Wuensch, Phys. Rev. ST Accel. Beams **12**(9), 092001 (2009).

- [16] B. Jüttner, *J. Phys. D: Appl. Phys.* **34**(17), R103-R123 (2001).
- [17] A. Anders, S. Anders, B. Jüttner, and H. Luck, *IEEE Trans. Plasma Sci.* **24** (February), 69-70 (1996).
- [18] A. Batrakov, N. Vogel, S. Popov, D. Proskurovsky, D. Kudimov, and D. Nikitine, *IEEE Trans. Plasma Sci.* **30** (February), 106-107 (2002).
- [19] P. Siemroth, T. Schulke, and T. Witke, *IEEE Trans. Plasma Sci.* **23** (December), 919-925 (1995).
- [20] Y. Levinsen, A. Descoedres, S. Calatroni, M. Taborelli, and W. Wuensch, Statistical modeling of dc sparks, in: Proceedings of the 23rd Particle Accelerator Conference (PAC 09), Vancouver, Canada, (2009), TU5PFP012.
- [21] K. Matyash, R. Schneider, F. Taccogna, A. Hatayama, S. Longo, M. Capitelli, D. Tskhakaya, and F.X. Bronold, *Contrib. Plasm. Phys.* **47** (December), 595-634 (2007).
- [22] D. Tskhakaya, K. Matyash, R. Schneider, and F. Taccogna, *Contrib. Plasm. Phys.* **47** (December), 563-594 (2007).
- [23] F. Bronold, K. Matyash, D. Tskhakaya, R. Schneider, and H. Fehske, *J. Phys. D: Appl. Phys.* **40**(21), 6583-6592 (2007).
- [24] H. Padamsee, J. Knobloch, and T. Hays, *RF Superconductivity for Accelerators* (Wiley Series in Beam Physics and Accelerator Technology, 1998).
- [25] R. Forbes, *Ultramicroscopy* **79**, 11-23(13) (September 1999).
- [26] J.W. Wang and G.A. Loew, *Part. Accel.* **30** (SLAC-PUB-5059), 225-230. 6 p (1989).
- [27] J. Hölzl, F. Schulte, and H. Wagner, *Solid Surface Physics*, Springer Tracts in Modern Physics, Vol. 85 (Springer Berlin / Heidelberg, 1979).
- [28] E.L. Murphy and R.H. Good, *Phys. Rev.* **102**(6), 1464-1473 (1956).
- [29] R.G. Forbes, *Appl. Surf. Sci.* **87-88**, 1-11 (1995), Proceedings of the 41st International Field Emission Symposium.
- [30] M. Vesely and G. Ehrlich, *Surface Science* **34** (February), 547-560 (1973).
- [31] A. Descoedres, A. Hansen, J. Kovermann, and H. Timko, Experimental results from the DC spark setup at CERN, (to be published), 2009.
- [32] S. Trajmar, W. Williams, and S.K. Srivastava, *J. Phys. B: At. Mol. Phys.* **10**(16), 3323-3333 (1977).
- [33] M.A. Bolorizadeh, C.J. Patton, M.B. Shah, and H.B. Gilbody, *J. Phys. B: At. Mol. Opt. Phys.* **27**(1), 175-183 (1994).
- [34] A. Aubreton and M. F. Elchinger, *J. Phys. D: Appl. Phys.* **36**(15), 1798-1805 (2003).
- [35] Y. Yamamura and H. Tawara, *At. Data Nucl. Data Tables* **62**, 149-253(105) (March 1996).
- [36] H. Timko, F. Djurabekova, K. Nordlund, L. Costelle, K. Matyash, R. Schneider, G. Arnau-Izquierdo, A. Descoedres, S. Calatroni, M. Taborelli, A. Toerklep, and W. Wuensch, Mechanism of surface modification in the plasma-surface interaction in electrical arcs, *Phys. Rev. B* **81**(18), 184109 (2010).
- [37] A. Anders and G.Y. Yushkov, *Surf. Coat. Technol.* **136**(1-3), 111-116 (2001).
- [38] B. Chapman, *Glow Discharge Processes Sputtering and Plasma Etching* (John Wiley & Sons, 1980).
- [39] B. Henrist, N. Hilleret, C. Scheuerlein, M. Taborelli, and G. Vorlaufer, The variation of the secondary electron yield and of the desorption yield of copper under electron bombardment: origin and impact on the conditioning of the LHC, in: Proceedings of the 8th European Particle Accelerator Conference (EPAC02), Paris, France, (2002).
- [40] K. Nakayama and J.H. Weaver, *Physical Review Letters* **82**(5), 980-983 (1999).
- [41] R.E. Johnson and J. Schou, *Matematisk Fysiske Meddelelser Konglige Danske Videnskabernes Selskab* **43**, 403-493 (1993).
- [42] C. Benvenuti, G. Canil, P. Chiggiato, P. Collin, R. Cosso, J. Guérin, S. Ilie, D. Latorre, and K.S. Neil, *Vacuum* **53**(1-2), 317-320 (1999).
- [43] P.A. Chatterton, *Proc. Phys. Soc.* **88**(1), 231-245 (1966).
- [44] A. Grudiev, S. Calatroni, and W. Wuensch, *Phys. Rev. ST Accel. Beams* **12**(10), 102001 (2009).
- [45] D.W. Williams and W.T. Williams, *J. Phys. D: Appl. Phys.* **5**(2), 280-290 (1972).
- [46] W. Wuensch, High-gradient breakdown in normal-conducting RF cavities, in: Proceedings of the 8th European Particle Accelerator Conference (EPAC 02), Paris, France, (2002), MOYGB003.
- [47] J.P. Barbour, W.W. Dolan, J.K. Trolan, E.E. Martin, and W.P. Dyke, *Phys. Rev.* **92**(1), 45-51 (1953).